PHYSICS

Diamond-based microwave quantum amplifier

Alexander Sherman, Oleg Zgadzai, Boaz Koren, Idan Peretz, Eyal Laster, Aharon Blank*

Amplification of weak microwave signals with minimal added noise is of importance to science and technology. Artificial quantum systems, based on superconducting circuits, can now amplify and detect even single microwave photons. However, this requires operating at millikelvin temperatures. Natural quantum systems can also be used for low-noise microwave amplification using stimulated emission effects; however, they generate a higher noise, especially when operating above ~1 K. Here, we demonstrate the use of electron spins in diamond as a quantum microwave amplifier operating with quantum-limited internal noise, even above liquid nitrogen temperatures. We report on the amplifier's design, gain, bandwidth, saturation power, and noise. This capability can lead the way to previously unavailable quantum science, engineering, and physics applications.

INTRODUCTION

The technology for amplification and detection of microwave (MW) signals with minimal addition of noise is critical to a variety of applications, such as deep-space communications, radio astronomy, radar, MW spectroscopy, and quantum technology (e.g., quantum computing, quantum sensing, and quantum communication). In these applications, the signal of relevance is very weak, sometimes at the level of tens to hundreds of MW photons per second. Therefore, any noise added to the signal during the amplification process might overwhelm it and eliminate the possibility of detecting it within a reasonable averaging time. Currently, three main types of amplifiers are used to amplify and subsequently possibly detect MW signals with very low addition of noise. (i) Conventional electronic amplifiers, predominantly based on high–electron mobility transistor (HEMT) semiconductor technology: They optimally operate at ~5 K or below and add ~10 noise photons to the signal in 1 s for 1-Hz bandwidth (*1*). (The number of noise photons per second is linear with the acquisition bandwidth.) (ii) Amplifiers based on superconducting circuits: These include the families of SQUID (superconducting quantum interference device)–based amplifiers, radio frequency single-electron transistors, and quantum Josephson parametric amplifiers (*2*), as well as the more recent Josephson traveling-wave parametric amplifier (*3*) and kinetic inductance parametric amplifiers (*4*). Such amplifiers typically operate at ~10 to 25 mK and make use of a variety of nonlinear phenomena occurring in superconductors to amplify MW signals with quantum-limited noise performance (e.g., adding 0.5 photons of noise per second for 1 Hz of bandwidth). (iii) Solid-state maser (MW amplification by stimulated emission of radiation) devices: These amplifiers rely on paramagnetic species, mainly ions embedded in a crystal such as ruby (Cr^{3+} in a crystal of Al_2O_3). Under an external static magnetic field, the paramagnetic species in the solid-state maser have at least three energy levels for their unpaired electrons (Fig. 1). One can use MW pumping to reach a state of population inversion in which there are more electrons in a higher energy level than in a lower one. Under such conditions, incoming MW radiation causes the stimulated emission of additional MW radiation—namely, the amplification of the incoming signals. Solid-state masers operate efficiently only at low temperatures (~1 K) and typically add a few photons of noise to the signal per second for 1-Hz bandwidth (*5*).

Until now, maser technology, developed in the 1950s and 1960s, was used mainly in niche yet important applications in space communication and radio astronomy [for example, detection of the black body radiation of the universe and remnant of the "big bang" (*6*)]. At present, it has been mostly abandoned in favor of the conventional electronic amplifiers mentioned above because of its complicated implementation, requirement for low operation temperature, and limited bandwidth/gain performance. When considering other external effects and peripheral system losses, NASA's recent publications state that in some cases the overall performance of HEMTs is superior to that of masers (*7*).

With the rising age of quantum technology, new scientific and technological endeavors are coming into play, requiring amplification of very weak MW signals with quantum noise–limited performance for applications ranging from the readout of quantum bits (*8*) to dark matter detection (*9*). These needs can currently be met only by the superconducting-based amplifier technology mentioned above, which necessitates the use of ultralow cryogenic temperatures that make its operation very complicated and limited in scope. It could be very beneficial to have a complementary technology for quantum noise–limited MW amplifiers that could be operated at much higher temperatures, even at room temperature. In that respect, modern maser technology may be the answer to this problem. The most recent and relevant effort in this direction is related to the use of paramagnetic color centers in diamond, called nitrogen-vacancy (NV) centers, as a basis for quantum MW oscillators (*10*). This experiment demonstrated that such a diamond system, when placed inside a very high-quality factor (Q) MW cavity, can generate continuous MW output while it is optically irradiated at room temperature to create a steady state of population inversion (Fig. 2). Unfortunately, this oscillator's limited output power (~−90 dBm) greatly limits its utility as a useful MW source and prevents the proper measurement of important oscillator parameters, such as frequency stability and phase noise. While the amplifying medium is in the solid state, the spins' low concentration makes this device's operational characteristics more akin to those of a gas-based maser (*11*). Moreover, although

Schulich Faculty of Chemistry, Technion-Israel Institute of Technology, Haifa 3200003, Israel.
*Corresponding author. Email: ab359@technion.ac.il

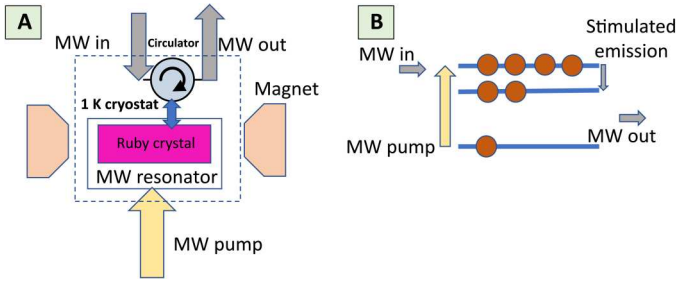

Fig. 1. Conventional solid-state maser. (**A**) Schematic overview of a conventional solid-state maser using a ruby single crystal embedded in an MW cavity and subjected to a static magnetic field. (**B**) Three relevant energy levels of a typical solid-state maser. The separation between levels is dictated by the strength of the static magnetic field, B_0. MW radiation is used to pump the levels and create population inversion, enabling stimulated emission also in the MW regime (albeit for lower energy than the pump's MW photons). This type of maser can operate well only at a temperature of ~1 K; at higher temperatures, all the levels are almost equally populated. In addition, the spin-lattice relaxation time, T_1, becomes too short to enable population inversion with reasonable pumping power.

theoretical works predicate that such diamond-based masers may also serve as quantum noise–limited amplifiers at ambient temperatures (*12*), the experimental efforts to date have not shown any actual amplification effects, making it impossible to measure any amplifier-related parameters (gain, bandwidth, noise, etc.).

Here, we take maser technology another substantial step forward and demonstrate with it an actual operational amplifier. Such a step required a complete rethinking and redesign of the concept described in the early work (*10*) to realize an actual useful device: a device whose amplification and noise properties could be measured, and which could be potentially implemented in various fields of MW technology and quantum science.

RESULTS

The new maser device

The general scheme of our new maser quantum amplifier is described in Fig. 3, and its full mechanical and electromagnetic details are provided in the Supplementary Materials (Materials and Methods). Our maser's concept and design are directed to achieve an MW amplifier with a reasonable gain of at least 20 dB, instantaneous bandwidth of ~10 MHz, and saturation input power of more than −60 dBm (1 nW) and, most importantly, to show quantum noise–limited performance at temperatures much higher than ~1 K, ideally reaching room temperature. To achieve these capabilities, it is necessary to carefully examine the expressions related to the operation and performance of maser devices. First, the device must reach the so-called "maser threshold," meaning that the MW losses of the cavity, including its coupling losses to the environment, are smaller than the net gain by the stimulated emission effect. In quantitative terms, this can be written as [(*13*), p. 254; (*14*), part 8]1

$$Q_{th} = Q_m \equiv \frac{1}{\eta\chi''} = \frac{8}{\eta\Delta n\mu_0\gamma^2\hbar T_2^*} \quad (1)$$

where Q_{th} is the minimum value for the quality factor of the cavity required to sustain maser self-oscillating action, Q_m is the quality factor due to the maser's gain medium (referred here in its absolute value, but actually having a negative value), and χ'' is the MW magnetic susceptibility of the NVs in the diamond at resonance. The terms μ_0 and γ are physical constants (free space permeability and electron gyromagnetic ratio factor, respectively), while T_2^* is related to the inverse spectral linewidth of the NV^-, Δf, by the expression $T_2^* = 1/\pi\Delta f$, and Δn is the population inversion difference between the upper and lower energy levels of the NV^- transition

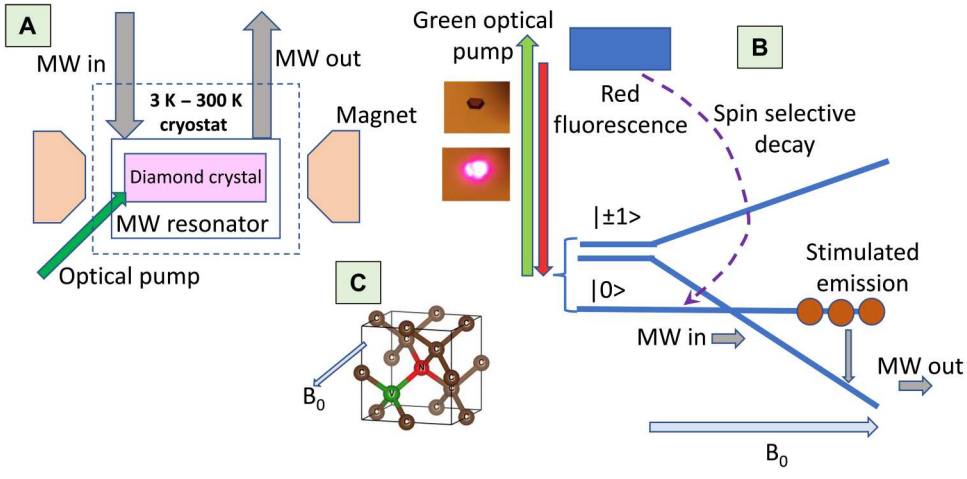

Fig. 2. Diamond-based maser. (**A**) Schematic overview of the diamond-based maser device operating at a wide range of temperatures with optical pumping. (**B**) Three lowest levels of the NV^- system, Zeeman splitted, and the optically excited states. At zero magnetic field, the $m_s = 0$ level (denoted as |0>) has a lower energy than the two degenerate $m_s = \pm1$ levels. Excitation by green light results in red fluorescence along with other nonradiative transitions, leading to an enhanced population of the |0> state. The application of a static magnetic field along the nitrogen-vacancy (NV) defect axis results in a population inversion between the |0> and |−1> states. In contrast to conventional solid-state masers, the selective population mechanism performs well even at room temperature. This is because the excited optical state is mostly empty even at that temperature, while the Zeeman levels' T_1 is still long enough. The spins' temperature, T_m, is negative in this case and can reach the quantum limit if $|T_m| < (h\nu/k_B)$. The inset on the left shows a photo of a typical synthetic diamond crystal processed in our laboratory to generate a high concentration of NV^- defects excited by green light giving out red fluorescence. (**C**) Atomic structure of an NV color defect in a diamond crystal. Such a defect is stable, and its negative state (NV^-) is paramagnetic with spin $S = 1$.

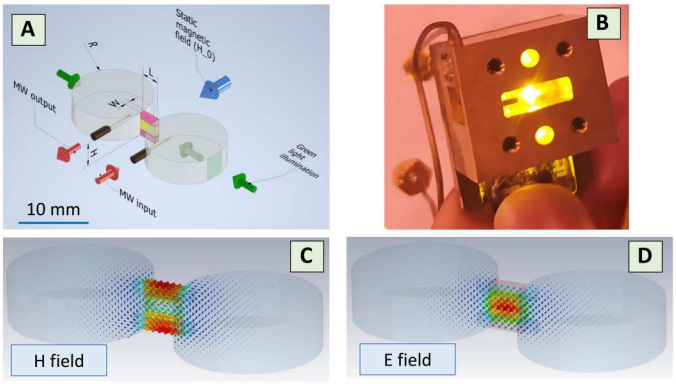

Fig. 3. The diamond-based maser amplifier. (**A**) Schematic overview of the custom-made maser cavity, which has two ports for the MW (in/out) and two optical windows for light irradiation. The two diamond crystals used for the amplification process are positioned at the center (purple), with an Al_2O_3 single crystal slab positioned between them (yellow). (**B**) Photograph of the central part of the maser cavity (with the outer portions removed) open on one side, with light irradiation from the opposite side emerging through the diamonds and the Al_2O_3 crystal. (**C**) Calculated MW magnetic field of the cavity's resonant mode with the diamonds and Al_2O_3 in it. The MW magnetic field is predominantly focused inside the diamond crystals. (**D**) Same as (C) but for the MW electric field, which is mainly focused inside the Al_2O_3 crystal.

used for maser amplification, per unit of volume. The term η denotes the filling factor and is defined as $\eta = \int_{\text{Diamond}} |\mathbf{B}_1^t|^2 / \int_{\text{Resonator}} |\mathbf{B}_1|^2$, where the nominator involves the size of the MW magnetic field component, $\mathbf{B}_1^t$, tangential to the direction of the static magnetic field, $\boldsymbol{B}_0$, and the denominator includes the size of the total MW magnetic field $\boldsymbol{B}_1$. An inspection of Eq. 1 reveals that there are four terms that can be controlled to some extent: the cavity's quality factor (Q), the spectral width of the spins (controlled via T_2^*), their population difference (Δn), and the filling factor (η). Accordingly, in our view, one can consider two different approaches for constructing a device that reaches the maser threshold. The first [type (i) maser device] calls for the use of a cavity with the highest possible Q factor and a relatively dilute material (small Δn), which, accordingly, has a narrow spectral line (long T_2^*) (*15*). In such a case, having even a small filling factor (small η) should be enough to produce sustained oscillations, as was demonstrated in (*10*). The price to pay when going in this direction is the limited bandwidth of operation, limited output power (implying limited saturation power, if aiming at an amplifier application), and, accordingly, limited gain (if at all). The alternative approach presented here [type (ii) maser device[is to use a cavity with a relatively low Q that supports a large bandwidth and achieves the maser threshold by a concomitant increase in NV concentration (Δn) along with a significant increase in the filling factor (η). The increase in NV concentration causes an increase also in the spectral width (T_2^* decreases), so the device has a larger bandwidth, as desired. The summary of the characteristics and performance of the type (i) maser device versus our type (ii) device is given in Table 1, which provides a quantitative comparison between the two approaches (see also the experimental results for more details on the data in Table 1).

Experimental data

The experiments conducted here considered two possible operational modes of the maser device: (i) as an oscillator and (ii) as an amplifier.

Maser oscillator

When operating the maser as an oscillator, it is best to reduce the coupling in its two MW ports; otherwise, the Q factor may be too low to comply with Eq. 1 ($1/Q = 1/Q_0 + 1/Q_{in} + 1/Q_{out}$, where Q_0 is the unloaded quality factor, and Q_{in} and Q_{out} relate to the coupling loses for the input and output ports, respectively). Therefore, for this experiment, we operated the maser cavity with only one output port connected to it ($Q_{in} = \infty$) and adjusted it to be under-coupled (see the S_{22} plot in Fig. 4) with −3-dB return loss so that the overall cavity Q is Q = 384 [voltage standing wave ratio (VSWR) = Q_{out}/Q_0 = 5.8]. The experiential setup for the maser oscillator measurements is shown in fig. S1A. First, we tried to observe maser oscillations at room temperature, but these attempts were unsuccessful. The presumed reasons for this are the cavity's low quality factor and the limited level of spin polarization available at such temperature, which is roughly 50 times lower than the maximum (see also the section titled "NV^- spin levels' population and relaxation times at various temperatures" in the Supplementary Materials). As temperature is reduced, the cavity's quality factor slightly improves and, most importantly, the spin polarization greatly increases (see table S2). Maser oscillations are first observed at ~100 K and below. Figure 5 shows the spectral power output of the free-running maser in an oscillator mode with the abovementioned coupling conditions, measured at 30 K, with total light irradiation power of ~1.4 W provided by each of the green light-emitting diodes (LEDs) (of which only ~1.5% actually reach the diamonds; see fig. S3 and related text). The typical power output for the maser oscillator ranges from ~−110 dBm at 78 K to ~−75 dBm at 30 K, whereas at 78 K it is slightly above the maser threshold for these coupling conditions. The maser frequency's 3-dB bandwidth typically ranges between 1 and 5 kHz, while for different traces (taken

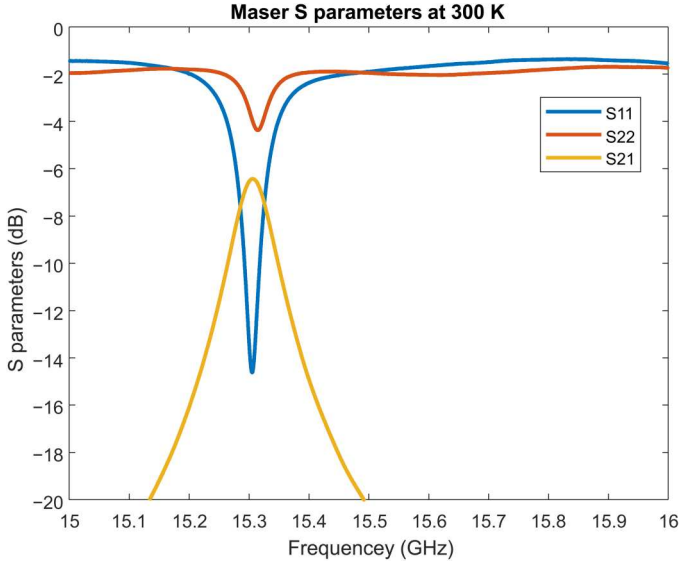

Fig. 4. The scattering matrix properties of the maser's cavity. S11 and S22 show two different coupling settings, while S21 is plotted when the input port is under-coupled and the output port is over-coupled.

Table 1. The main characteristics and operational parameters of the two maser devices are described (*10*) and in this work. Certain parameters of the high *Q* approach were not explicitly reported and therefore are calculated here, based on the provided data (marked with an asterisk).

Parameter	(i) High *Q* approach	(ii) Low *Q* approach
Unloaded *Q* (denoted as Q_0)	55,000	450
NV population difference, Δn (only the part that contributes to the maser signal)	~3.5×10^{15} cm^{-3}	6.2×10^{17} cm^{-3}
Spins' linewidth Δf	610 kHz	9.1 MHz
Filling factor	0.0132*	0.433
Output power as an oscillator	Less than −90 dBm	More than −75 dBm
Output power as an amplifier	–	More than −47 dBm
Small signal gain	–	More than 20 dB
Amplifier's bandwidth	–	~0.5–6 MHz (depending on input power)
Amplifier's internal noise temperature	–	~0.7 K (quantum limited)
Operation as an oscillator	+	+
Operation as an amplifier	–	+
Operating temperature range	Data at ~297 K	5–120 K
Spins' temperature, $\lvert T_m \rvert$	1.2 K*	→ 0 K
Maser quality factor, Q_m	28,132*	212
Oscillator linewidth output limit	50 Hz	210 Hz

every ~10 s) this frequency jumps in the range of a few hundreds of kilohertz (Fig. 5). The magnetic field stability of our electromagnet in this time frame [measured by monitoring the electron spin resonance (ESR) signal of a narrow-linewidth radical] is on the order of ~0.1 G, corresponding to frequency variations of ~280 kHz, which is the likely cause of these jumps. The field drifts are also possibly the cause of the relatively large instantaneous bandwidth seen for a given trace. It is expected that a setup with improved electromagnet stability, and better even—a permanent magnet, would significantly enhance the stability of the maser oscillator. Furthermore, the onset point of the maser's self-oscillations, along with measurements of the cavity's quality factor, enables us to provide a good estimate for the Q_m value of the maser with full light pumping (corresponding to full population inversion, as we obtain below 100 K; see table S2), which is Q_m = ~300. Q_m is a critical parameter for determining much of the maser's performance as an amplifier [(*16*), see also the following subsection]. The experimental estimate for Q_m can be compared to the expected value, as calculated by Eq. 1, using the parameters shown in Table 1 (T_2^* = 35 ns, $\Delta n = 6.2 \times 10^{23}$ spins/m^3, η = 0.433), leading to Q_m = ~212. Given the uncertainties in the experimental estimation of Q_m, the uncertainties in NV^- concentration, the irregular shape of the

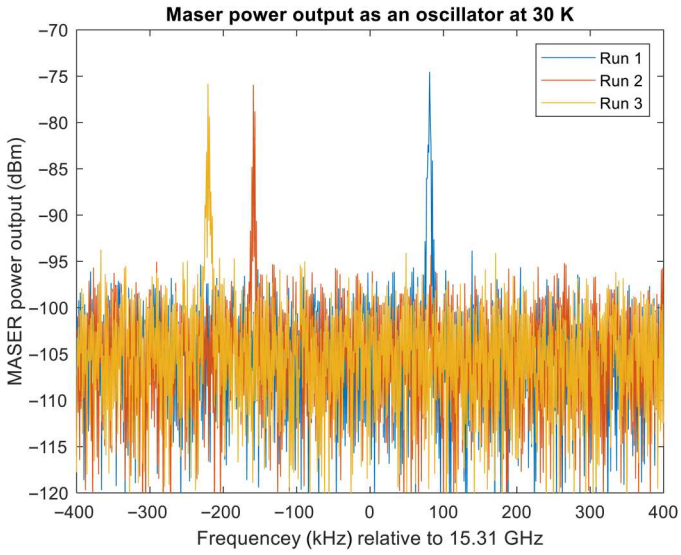

Fig. 5. The output of the maser as an oscillator. The plot shows three different traces taken at ~10-s intervals. The spectrum analyzer's resolution bandwidth is 1 kHz.

diamonds and Al_2O_3 crystal we used here, and the production tolerance of the metallic cavity, the two results are in fair agreement and provide much insight about the current capabilities and the potential of this technology (see Discussion).

Maser amplifier

When operating the maser as an amplifier, its gain, bandwidth, saturation power, and noise characteristics are heavily dependent on the coupling properties of its input and output ports [(*16*), pp. 262 and 396]. In the case of the two-port maser, it is recommended to have critical coupling in the input port and to undercouple the output port. The S_{11}, S_{22}, and S_{12} plots of the maser cavity under these coupling conditions are shown in Fig. 4.

Maser's gain and bandwidth. Figure 6 presents the gain of the maser device versus input frequency, for various input power levels, at temperatures of 30 and 78 K. The maser's small signal (<−90-dBm input) gain reaches more than 20 dB at 30 K but only ~6 dB at 78 K. The bandwidth is ~0.5 MHz for the high gain at 30 K and increases up to ~5 MHz for the small gain at 78 K. Overall, the voltage gain × bandwidth is ~5.8 ± 0.5 MHz for all power levels at 30 K and ~5.3 ± 0.5 MHz at 78 K (the voltage gain is calculated as the square root of the power gain).

Maser's noise. The noise temperature of the maser amplifier is evaluated here using two methods: (i) based on the measured population of the NVs' Zeeman levels under light irradiation (or, equivalently, Q_m) and (ii) by direct measurements using an MW noise source with two different noise temperature levels [(*16*), p. 404]. Let us first refer to method (i) and then compare it to the results of the direct measurements obtained by method (ii). The noise temperature of a transmission cavity maser is given by [(*16*), p. 396]

$$T_a = \lvert T_m \rvert \frac{1}{1-\varepsilon} + T_0 \frac{Q_l}{Q_0} + T_L \frac{\varepsilon}{1-\varepsilon} \quad (2)$$

where T_m is the equivalent thermodynamic temperature of the pumped spin system of the maser, T_0 is the physical temperature of the cavity, and T_L is the physical temperature of the load at the output. The coupling factor is defined as $\varepsilon \equiv Q_m/Q_2$, and for high

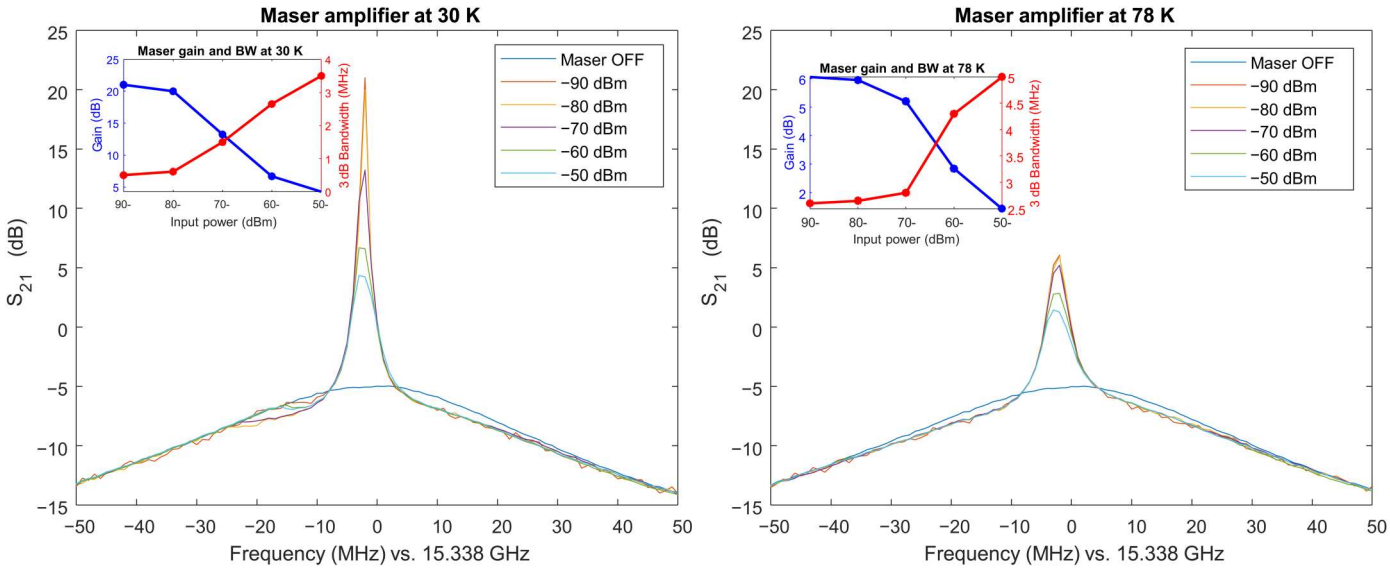

Fig. 6. The maser as an amplifier. The maser amplifier's gain at 30 K (left) and 78 K (right) for various input power levels. When the maser is OFF, there is a ~5-dB loss for signals going through the device due to the coupling properties of its ports (the main loss is due to the undercoupled output port). The insets show the maser's power gain and 3-dB bandwidth (BW) at these two temperatures.

gain settings, $1 - \varepsilon \approx Q_m/Q_1$. In principle, the noise contribution from the load (the third term on the right) can be greatly reduced using a cold isolator at the output. However, since we aim to operate our maser device with loads at elevated temperatures (possibly even at room temperature), it would be advisable to eliminate the load contribution to the noise as much as possible by undercoupling the output port ($\varepsilon << 1$). This setting also minimizes the noise contribution from the cavity itself (because, under these conditions, Q_1 is set to be $\sim Q_m << Q_0$), which, again, is important if we wish to operate the maser at elevated temperatures. The "only" problem in choosing a small coupling factor is that the gain × bandwidth term, which is proportional to $\sqrt{\varepsilon(1-\varepsilon)}$, is reduced. A reasonable compromise may involve choosing $\varepsilon = \sim 0.1$ so that the gain-bandwidth product drops only by a factor of ~3. For the calculated $Q_m = \sim 212$, as described above, we obtain $Q_1 = \sim 235$ and $Q_0 = \sim 450$. Namely, with Eq. 2, we obtain $T_a = 1.1 \times T_m + 0.52 \times T_0 + 0.11 \times T_L$. The maser's spins' temperature, $|T_m|$, is found by measuring the degree of population inversion in our system (see table S2) and is quantum-limited to $h\nu/k_B \sim 0.73$ K. Thus, under our experimental conditions, for the maser operating at 30 K connected to a cold isolator at 38 K (table S1), we obtain $T_a = 20.6$ K. In practice, as noted above, Q_m is experimentally found to be ~300, which means that the effect of the cavity's temperature is much more pronounced, and we get $T_a = 1.1 \times T_m + 0.73 \times T_0 + 0.11 \times T_L \sim 26.9$K.

Going over now to method (ii), the noise temperature of our maser device was directly measured using the Y-factor method (*17*), with the setup shown in fig. S1B. The measurement was carried out by comparing the device's noise level output when the noise source is OFF (emitting just regular thermal noise) to the level when the noise source is ON (emitting a 40-times larger noise power, in our case) and using the expression

$$T_a = \frac{T_{g2} - rT_{g1}}{r-1} - \frac{T_a'}{G} \quad (3)$$

where T_{g2} and T_{g1} are the equivalent noise temperatures at the maser's input port when the noise source is ON and OFF, respectively; r is the noise power ratio measured in the spectrum analyzer between these two cases; T_a' is the noise temperature of the receiver after the maser (found to be 336 ± 66 K; see table S1); and G is the maser's gain. Table S1 presents the noise and loss parameters of our setup for maser operation at 30 K, out of which the values of T_{g1} and T_{g2} were calculated (see also details in the Supplementary Materials); these were found to be 55.8 ± 1.1 K and 528.5 ± 22.4 K, respectively (table S1). The parameter r was measured to be 6.3 ± 0.3, which leads to the result (using Eq. 3) of T_a = 30.7 ± 8.5 K. A similar analysis of the maser's experimental data at 78 K leads to T_a = 95.3 ± 15.2 K.

DISCUSSION

The results of the new maser device are now discussed with respect to its two modes of operation, as an oscillator and as an amplifier. We compare our results to analytical predictions as well as to a numerical simulation we developed for calculating the maser's main operational parameters (see the Supplementary Materials).

Maser oscillator

While the maser oscillator was not our main aim in this work, its results are important to understand the current properties and limitation of the maser amplifier and its technology. The main outcomes of the oscillator experiments are data about the maser's output power, which was measured with good accuracy, and the observation of the oscillation threshold, enabling us to estimate Q_m. Unfortunately, because of magnetic field instabilities, the maser oscillator's linewidth could not be measured well, and its phase noise properties were not measured at all. The output power should ideally correspond to a situation in which, for each optical photon of the pump signal, we obtain an MW photon. Given our use of optical pumping of ~0.7 W per LED, ideally, we can expect a maximum oscillator output of −23 dBm (also considering that only

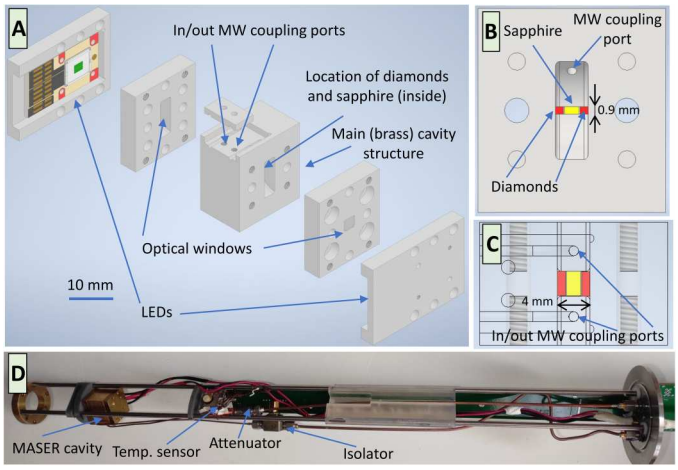

Fig. 7. The maser's cavity structure. (**A**) Exploded isometric view of the cavity structure. (**B**) Cross section of the cavity viewed from the direction of the light illumination. (**C**) Cross section of the cavity structure viewed from the top. (**D**) A photograph of the assembled cryogenic probe head with the maser cavity in it.

one of four NVs are in the right orientation). In practice, because of the light irradiation geometry (Fig. 7 and fig. S3), a much lower optical power actually reaches the diamonds, and many photons are absorbed by other defects in the diamond. A better estimation of the maximum available power from our maser oscillator setup can be obtained by optimal simulation of the light inside the cavity that takes into account the exciting optical power density and its angle dependence, the optical absorption cross section of the NVs, their concentration, the cavity volume, etc. (see the Supplementary Materials). Using this simulation, we obtain an expected maximum output power of ~−60 dBm. This is still greater than the measured ~−73-dBm output; however, we believe that this discrepancy is mainly due to additional issues with the setup's light irradiation inefficiency that could not be simulated, as well as to the magnetic field fluctuations that smear out the expected maser oscillator's sharp line. This linewidth of the maser oscillator should ideally reach the Schawlow-Townes limit (*18*) of $\Delta\nu_{\mathrm{MASER}} = \frac{4\pi h\nu}{P_{\mathrm{out}}}(\Delta f)^2 \sim 210[\mathrm{Hz}]$ for the maximum output power we observed of ~−73 dBm. We estimate that with a much more stable static magnetic field setup, the output power and the linewidth would be significantly larger and smaller, respectively. These field drifts also make it very hard to measure the phase noise of the maser source. It is thus evident that to enable real applications of the maser as an MW source and to properly measure the phase noise of such an oscillator, one must use much more stable magnets, preferably based on permanent magnets that have excellent short-term (in the range of seconds) field stability (*19*). This mainly technical issue can be resolved, potentially resulting in a unique narrowband MW source with high short-term (<1 s) stability and very low phase noise, similar to other state-of-the-art cryogenic MW sources (*20*). Such a source could operate at considerably higher temperatures. [A related concept of maser-based oscillators, operating only at cryogenic temperatures, can be found in (*21*).] A recent discussion of additional prospects and applications of diamond-based maser oscillators can be found in (*22*). The most relevant is the potential use in diamond-based sensitive magnetometry (*23*), where it is possible to boost sensitivity even further due to the extended coherent probing time it provides compared to nonmasing devices. [Masers continue to oscillate coherently for a much longer time than the native coherence time, T_2, of the spins, which enables a much more sensitive magnetometry (*24*).]

Maser amplifier

In this work, we were able to operate the diamond maser in amplifier mode and, accordingly, evaluate all of its relevant parameters. We can thus compare the maser amplifier's measured parameters to the theoretical predictions.

1) The voltage gain-bandwidth product of the maser was experimentally found to be up to 5.8 MHz, which is comparable to the expected theoretical value of $g_0\Delta f = \frac{2}{Q'_{\mathrm{m}}} f\,[\varepsilon(1-\varepsilon)]^{1/2} \sim 12.2\mathrm{MHz}$ [(*16*), p. 262], where g_0 is the voltage gain, Δf is the amplifier 3-dB power bandwidth, and $1/Q'_{\mathrm{m}} = 1/Q_{\mathrm{m}} - 1/Q_0$. However, the analytical expression is approximate and not very accurate under our conditions of $|Q_{\mathrm{m}}|$, which is not much smaller than Q_0. Our more exact numerical simulation (see the Supplementary Materials) leads to a gain-bandwidth product of ~7.8 MHz, which is closer to what we see in practice.

2) The expected saturation power of the maser as an amplifier can also be evaluated using our numerical simulation and was found to be −55 dBm. This is comparable to the >−47-dBm output we obtained in the experiment (gain of ~3 dB for −50-dBm input), with the small discrepancy possibly attributed to the slight increase in Q_0 at lower temperatures, which would improve the simulated values and the possible slight increase in optical power efficiency, also due to the lower temperatures.

3) The maser's noise temperature was evaluated using two different methods, both leading to a total maser amplifier noise temperature of T_{a} = ~30 K when operating at 30 K. The dominant term in the maser amplifier's noise originated in cavity losses that were not cancelled well enough because of the relatively high Q_{m} (~300) that we achieved, which is not much smaller than Q_0, as optimally desired (Eq. 2). The maser's internal spin noise is quantum-limited, based on the pulsed ESR data that provided the spins' level populations (table S2), which shows that only the |0> level is populated.

Prospects and general conclusions

This work demonstrated the operation of a solid-state maser amplifier with quantum-limited internal noise at temperatures above liquid nitrogen. However, there is still much room for improvement to make this device useful for modern applications. The most critical issue is to improve (namely, reduce) the Q_{m} value. This can be achieved by increasing the NV^- concentration and making additional improvements in the filling factor via structural enhancements resulting in a better fit of the diamonds inside the cavity. In addition, a slight increase in the cavity's Q_0 would also help the noise performance without limiting the amplifier's bandwidth. However, we already work at very high NV concentrations [~14 parts per million (ppm)], which may maximally be increased by a factor of 2 without significantly degrading the transparency of the diamond and reducing optical pumping efficiency. Moreover, the filling factor cannot be increased much more because it is already nearing unity value. Thus, as a practical limit, such an optimized system would have Q_{m} of ~50 and Q_0 of ~1000. [Having a diamond with NV^- oriented only along the [111] direction (*25*) would further improve Q_{m} by an additional factor of 4, but this

technology is currently not available for such high NV concentrations and in bulk diamonds.] Under such conditions, the ambient temperature's contribution to the noise would be smaller or comparable to the maser's internal noise up to temperatures of ~20 K, and thus, up to such temperature, the device can serve as a true quantum-limited amplifier. In principle, our maser device can be operated at much higher temperatures than shown here. This would require a much more efficient light irradiation scheme that enables a high population inversion with much smaller pumping power. We have shown recently that it is possible to achieve almost full population inversion, even at room temperature, with a favorable light excitation geometry (*26*). One can approach a state of $T_m \to 0$, even at room temperature, although the maser's total noise as an amplifier is still larger, as expected from Eq. 2.

How does such a device compare to the current technologies for cryogenic low-noise MW amplification? Regarding HEMTs, the diamond maser device can exhibit quantum-limited amplification performance and thus would have superior noise performance for operations at similar frequencies and temperatures (<20 K). Moreover, unlike HEMTs, masers are not damaged by high-power MW pulses, which are of importance for applications such as communications, radar, and pulsed magnetic resonance. However, our maser device is clearly inferior to HEMTs in terms of bandwidth, output power, and system complexity. As noted above, operations at elevated (even room) temperatures require achieving high population inversion, which is feasible. However, any losses in the input would lead to increased noise in the amplifier. While at low frequencies of ~1 GHz such losses can be minimized (*27*), at higher frequencies, above 10 GHz, this becomes much harder and, ideally, one should pursue waveguide-based structures leading directly to the amplifier. Here, again, maser technology may be superior to HEMTs since cavity-type structures like the one we developed in this work are more amenable to enabling direct waveguide coupling with minimal losses (which would lead to noise).

Compared to amplifiers based on superconducting circuits, one obvious advantage of diamond maser technology is the possibility to provide quantum-limited amplification at much higher temperatures. In terms of gain, bandwidth, and saturation power, maser technology seems to be on par with the cavity-based superconducting circuits for the two first parameters and superior for the last one, providing much higher saturation power. Moreover, as noted above, masers are also not prone to damage by high-power MW pulses. If we compare them to the more recent traveling-wave parametric amplifiers, the latter are much more complex but have a much better gain and bandwidth than cavity-based superconducting devices. Still, it is fair to say that a similar diamond-based traveling-wave maser technology could be developed in the future, as was done for conventional solid-state masers (*28*). Such traveling-wave masers have significantly better bandwidth and gain compared to cavity-based designs but, again, at the expense of system complexity.

As a final note, it should be mentioned that because of the extremely high filling factor, high NV^- concentration, and strong spin-cavity coupling of our device, our experimental system exhibits a wealth of nonlinear effects, such as multiple echoes (*29*, *30*) and superradiance (*31*), that were observed even close to room temperature. Such phenomena were recently noted as important for research in the field of cavity quantum electrodynamics (*32*) and will hopefully be reported soon in another publication.

MATERIALS AND METHODS

Diamond single crystals

Diamond single crystals were purchased from Chenguang Machinery & Electric Equipment Co. Ltd., China. The diamonds are produced using the high-pressure–high-temperature technique. They are shaped as hexagons with nonequal edges (see, for example, the photo in the inset of Fig. 2B), with a typical edge length of ~2 to 3 mm. Their thickness is typically ~0.9 mm with a crystallographic face orientation of [1 1 1]. The concentration of nitrogen impurities in the diamonds is specified by the producer to be ~100 to 200 ppm (the diamonds are not homogeneous). The more relevant parameter for the maser's operation is the concentration of the substitutional nitrogen [known as paramagnetic P1 centers (*33*)], which affects the value of the NVs' T_2^* and is the primary source of NVs. We measured the average concentration of the P1 centers and found it to be ~50 to 100 ppm. To that end, we used continuous-wave ESR (Bruker's X-band EMX system) and compared the diamond's ESR spectrum to that of a reference sample with a known number of spins. The native concentration of the NVs in the diamond is very low (less than 0.1 ppm), and therefore, they were irradiated by a beam of electrons (5 MeV) to a dose of 2×10^{19} electrons/cm^2 (at Sorvan Ltd., Yavneh, Israel) to convert the P1s to NVs. The irradiation was carried out in two phases. The first 101 irradiation hours were performed without heating, and an additional 81 hours of irradiation were performed while heating to about 650° to 750°C. The diamonds were kept in a vacuum in sealed quartz tubes during the irradiation procedure. Following this, the diamonds were cleaned using a boiling solution of nitric (68%), sulfuric (98%), and perchloric (70%) acids (1:1:1 ratio) for 1 hour. After this stage, the diamonds were cut by laser into pieces measuring 0.9 mm × 1.1 mm × 3 mm and cleaned again with acid. Cleaning the diamonds from any residues of carbonization is important to reduce the dielectric losses, which decrease the Q of the cavity. The clean carbonization-free diamonds were measured by us to have a loss tangent of $\delta \asymp 0.015$. This was done by measuring the Q factor of our cavity as a function of diamond's size and volume, and comparing the results to those calculated by finite element software (CST Microwave Studio). The concentration of the NVs in the diamond pieces used in the maser device was found to be ~14 ppm. This was measured using pulsed ESR Hahn echo field sweeps (by means of a pulsed ESR spectrometer by Spinflex, Israel) and comparing the NV signal to that of the P1s (see Fig. 8 for the NV spectrum). The same field-swept echo data were also used to evaluate the NVs' T_2^*, which was found to be ~35 ns.

Maser cavity and cryogenic probe

The design of the MW cavity aims to increase the filling factor, η, as much as possible, and to reach the highest possible Q values (but lower than ~1000 to avoid limiting the amplifier's bandwidth). It should also enable the efficient coupling of light into the cavity to maintain high levels of population inversion (Δn). The design also supports a variable MW coupling scheme and has a minimal mechanical width to allow it to be inserted into the gap of a compact magnet. To comply with all these requirements, we came up with the general design shown in Fig. 3 and in Fig. 7 below. The cavity's body is made from gold-plated cartridge brass and contains two diamond crystals and one crystal of sapphire (Al_2O_3), placed in

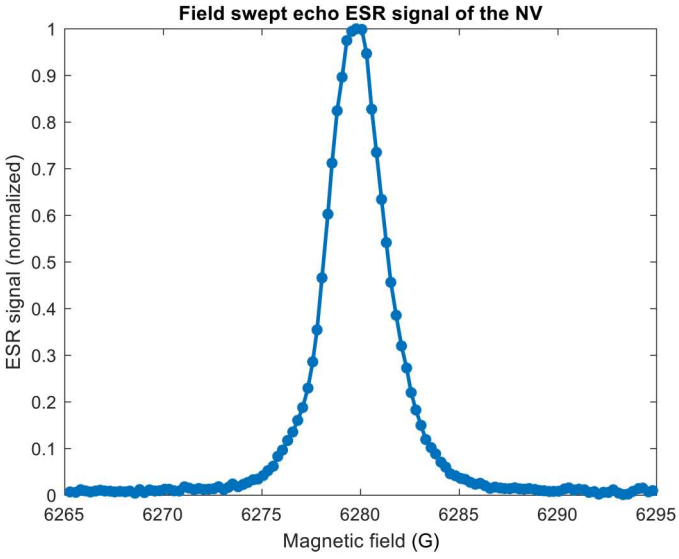

Fig. 8. ESR spectrum of the NVs. Field-swept Hahn echo spectrum of the NVs in the maser device, measured at 30 K, showing the |0>↔|−1> spin levels' transition. The superimposed Gaussian line fit has full width at half maximum (FWHM) of ~9.1 MHz, corresponding to T_2^* of ~35 ns.

a rectangular void that is extended by two cylindrical cavities forming an oval-like Cassini shape. This shape supports a cavity mode designed to localize and concentrate the MW magnetic field distribution, B_1, inside the diamond crystals, which serves to maximize the cavity filling factor η. Although in principle it would be best to fill the rectangular void completely with the diamond crystals, our design incorporates at the center of the void a sapphire (Al_2O_3) single crystal that has a higher permittivity than the diamond (~9.5 versus ~5.68) and thus focuses into it the MW electric field and thereby minimizes the diamonds' dielectric losses (see Fig. 3, C and D). While this causes a certain reduction in η compared to the case of having only diamonds in the void, such configuration maximizes the Qη product, which is the parameter of greatest relevance to our work (see Eq. 1). Moreover, smaller diamonds can be better excited by light illumination. The proposed design inherently supports both a single-port configuration best suited for signal generation applications (MW oscillator) and a two-port configuration (MW amplifier). The latter is realized by two coaxial lines protruding into the cylindrical sections of the cavity, which are used to couple the cavity's mode energy directly in/out of the cavity. The level of coupling can be determined by adjusting the length of the protruding sections. The light is supplied by two LEDs (model LE CG P2AQ from Osram Ltd.) positioned at both ends of the cavity that transmit light through a window in the cavity structure. These LEDs' irradiation spectrum is predominantly green (see fig. S4). They are driven by an Agilent E3644A power supply with current noise ripple of ~1% at the nominal 0.4 A used to drive the LEDs. While the cavity shown here operates at ~16 GHz, the same cavity concept can be designed to operate at other frequencies simply by changing the radius of the Cassini shapes, and/or the dimensions of the central block, and/or the size or permittivity of the central dielectric slab. The maser's cavity is integrated within a complete cryogenic probe head (Fig. 7D) that fits into a He-flow cryostat (Janis, USA, STVP-200). Figure 4 shows the S_{11} and S_{21} plots of our maser device measured at room temperature using a vector network analyzer (Keysight model N5224B). On the basis of these measurements, we can calculate the cavity's internal (unloaded) Q factor to be Q_0 = ~450.

Supplementary Materials

This PDF file includes:

Texts S1 to S5
Figs. S1 to S4
Tables S1 and S2
References

REFERENCES AND NOTES

1. M. W. Pospieszalski, Extremely low-noise cryogenic amplifiers for radio astronomy: Past, present and future, in *2018 22nd International Microwave and Radar Conference (MIKON)* (IEEE, 2018), pp. 1–6.
2. X. Gu, A. F. Kockum, A. Miranowicz, Y.-x. Liu, F. Nori, Microwave photonics with superconducting quantum circuits. *Phys. Rep.* **718–719**, 1–102 (2017).
3. C. Macklin, K. O'Brien, D. Hover, M. E. Schwartz, V. Bolkhovsky, X. Zhang, W. D. Oliver, I. Siddiqi, A near-quantum-limited Josephson traveling-wave parametric amplifier. *Science* **350**, 307–310 (2015).
4. D. J. Parker, M. Savytskyi, W. Vine, A. Laucht, T. Duty, A. Morello, A. L. Grimsmo, J. J. Pla, Degenerate parametric amplification via three-wave mixing using kinetic inductance. *Phys. Rev. Appl.* **17**, 034064 (2022).
5. M. S. Reid, *Low-Noise Systems in the Deep Space Network* (Deep-Space Communications and Navigation Series, Wiley, 2008).
6. A. A. Penzias, R. W. Wilson, A measurement of excess antenna temperature at 4080 Mc/s. *ApJ* **142**, 419–421 (1965).
7. J. J. Bautista, Deep space network, cryogenic HEMT LNAs (Jet Propulsion Laboratory, National Aeronautics and Space Administration, 2006); http://hdl.handle.net/2014/40245.
8. Z. R. Lin, K. Inomata, W. D. Oliver, K. Koshino, Y. Nakamura, J. S. Tsai, T. Yamamoto, Single-shot readout of a superconducting flux qubit with a flux-driven Josephson parametric amplifier. *Appl. Phys. Lett.* **103**, 132602 (2013).
9. K. M. Backes, D. A. Palken, S. A. Kenany, B. M. Brubaker, S. B. Cahn, A. Droster, G. C. Hilton, S. Ghosh, H. Jackson, S. K. Lamoreaux, A. F. Leder, K. W. Lehnert, S. M. Lewis, M. Malnou, R. H. Maruyama, N. M. Rapidis, M. Simanovskaia, S. Singh, D. H. Speller, I. Urdinaran, L. R. Vale, E. C. van Assendelft, K. van Bibber, H. Wang, A quantum enhanced search for dark matter axions. *Nature* **590**, 238–242 (2021).
10. J. D. Breeze, E. Salvadori, J. Sathian, N. M. Alford, C. W. M. Kay, Continuous-wave room-temperature diamond maser. *Nature* **555**, 493–496 (2018).
11. J. P. Gordon, H. J. Zeiger, C. H. Townes, The maser—New type of microwave amplifier, frequency standard, and spectrometer. *Phys. Rev.* **99**, 1264–1274 (1955).
12. L. Jin, M. Pfender, N. Aslam, P. Neumann, S. Yang, J. Wrachtrup, R.-B. Liu, Proposal for a room-temperature diamond maser. *Nat. Commun.* **6**, 8251 (2015).
13. A. E. Siegman, *An Introduction to Lasers and Masers* (McGraw-Hill Series in the Fundamentals of Electronic Science, McGraw-Hill, 1971), pp. xiii, 520 pp.
14. A. Yariv, *Quantum Electronics* (Wiley, 1967), pp. xvi, 478 pp.
15. J. A. van Wyk, E. C. Reynhardt, G. L. High, I. Kiflawi, The dependences of ESR line widths and spin-spin relaxation times of single nitrogen defects on the concentration of nitrogen defects in diamond. *J. Phys. D Appl. Phys.* **30**, 1790–1793 (1997).
16. A. E. Siegman, *Microwave Solid-State Masers* (McGraw-Hill Electrical and Electronic Engineering Series, McGraw-Hill, 1964), pp. xv, 583 pp.
17. Agilent, https://testworld.com/wp-content/uploads/noise-figure-measurement-accuracy-the-y-factor-method.pdf.
18. A. L. Schawlow, C. H. Townes, Infrared and optical masers. *Phys. Rev.* **112**, 1940–1949 (1958).
19. F. Hakelberg, P. Kiefer, M. Wittemer, T. Schaetz, U. Warring, Hybrid setup for stable magnetic fields enabling robust quantum control. *Sci. Rep.* **8**, 4404 (2018).
20. S. Grop, P. Y. Bourgeois, R. Boudot, Y. Kersalé, E. Rubiola, V. Giordano, 10 GHz cryocooled sapphire oscillator with extremely low phase noise. *Electron. Lett.* **46**, 420–422 (2010).
21. M. Mrad, Y. Kersalé, P. Bourgeois, V. Giordano, S. Grop, K. Benmessaï, M. Tobar, Recent progress on cryogenic MASER oscillator, in *2012 European Frequency and Time Forum* (IEEE, 2012), pp. 83–86.
22. D. M. Arroo, N. M. Alford, J. D. Breeze, Perspective on room-temperature solid-state masers. *Appl. Phys. Lett.* **119**, 140502 (2021).

23. J. F. Barry, J. M. Schloss, E. Bauch, M. J. Turner, C. A. Hart, L. M. Pham, R. L. Walsworth, Sensitivity optimization for NV-diamond magnetometry. *Rev. Mod. Phys.* **92**, 015004 (2020).
24. C. L. Degen, F. Reinhard, P. Cappellaro, Quantum sensing. *Rev. Mod. Phys.* **89**, 035002 (2017).
25. C. Osterkamp, M. Mangold, J. Lang, P. Balasubramanian, T. Teraji, B. Naydenov, F. Jelezko, Engineering preferentially-aligned nitrogen-vacancy centre ensembles in CVD grown diamond. *Sci. Rep.* **9**, 5786 (2019).
26. A. Sherman, L. Buchbinder, S. Ding, A. Blank, Performance analysis of diamond-based masers. *J. Appl. Phys.* **129**, 144503 (2021).
27. S. Weinreb, J. Shi, Low noise amplifier with 7-K noise at 1.4 GHz and 25 °C. *IEEE Trans. Microw. Theory Tech.* **69**, 2345–2351 (2021).
28. R. W. DeGrasse, E. O. Schulz-Dubois, H. E. D. Scovil, The three-level solid state traveling-wave maser. *Bell Syst. Tech. J.* **38**, 305–334 (1959).
29. K. Debnath, G. Dold, J. J. L. Morton, K. Mølmer, Self-stimulated pulse echo trains from inhomogeneously broadened spin ensembles. *Phys. Rev. Lett.* **125**, 137702 (2020).
30. S. Weichselbaumer, M. Zens, C. W. Zollitsch, M. S. Brandt, S. Rotter, R. Gross, H. Huebl, Echo trains in pulsed electron spin resonance of a strongly coupled spin ensemble. *Phys. Rev. Lett.* **125**, 137701 (2020).
31. A. Angerer, K. Streltsov, T. Astner, S. Putz, H. Sumiya, S. Onoda, J. Isoya, W. J. Munro, K. Nemoto, J. Schmiedmayer, J. Majer, Superradiant emission from colour centres in diamond. *Nat. Phys.* **14**, 1168–1172 (2018).
32. Y. Zhang, Q. Wu, S.-L. Su, Q. Lou, C. Shan, K. Mølmer, Cavity quantum electrodynamics effects with nitrogen vacancy center spins coupled to room temperature microwave resonators. *Phys. Rev. Lett.* **128**, 253601 (2022).
33. F. Jelezko, J. Wrachtrup, Single defect centres in diamond: A review. *Phys. Status Solidi A Appl. Mater. Sci.* **203**, 3207–3225 (2006).
34. M. Drake, E. Scott, J. A. Reimer, Influence of magnetic field alignment and defect concentration on nitrogen-vacancy polarization in diamond. *New J. Phys.* **18**, 013011 (2016).
35. C. M. Caves, Quantum limits on noise in linear amplifiers. *Phys. Rev. D* **26**, 1817–1839 (1982).

Acknowledgments: We thank A. Hoffman of ICDAT for assisting us in the diamonds' laser cutting and IAI ELTA Systems for its support in this research. **Funding:** This project was funded by the Israel Science Foundation (ISF), grant no. 1357/21, and the Israel Innovation Authority, grant no. 67697. **Author contributions:** All authors discussed the results and approved the manuscript. A.B. and A.S. conceived the project. A.S., O.Z., A.B., B.K., E.L., and I.P. carried out the methodological experimental work. A.S. and A.B. prepared the figure visualization. Funding was acquired by A.B., who also supervised the research. The original draft was written by A.B. and A.S., and the final review and editing was carried out by A.B., B.K., and A.S. **Competing interests:** A.S. and A.B. have a pending patent application named "Microwave quantum device" (application number US20220155243A1) related to diamond-based maser devices. The application was filed by the Technion Research and Development Foundation on 18 November 2021. **Data and materials availability:** All data needed to evaluate the conclusions in the paper are present in the paper and/or the Supplementary Materials. Additional software used to simulate and analyze the results are deposited in Zenodo: doi 10.5281/zenodo.7240947 and 10.5281/zenodo.7240951.

Submitted 30 August 2022
Accepted 3 November 2022
Published 7 December 2022
10.1126/sciadv.ade6527